

Low-Mass Neutron Stars with Rotation

A.V. Yudin^{1,2*}, T.L. Razinkova¹, S.I. Blinnikov^{1,3}

¹*Institute for Theoretical and Experimental Physics, ul. Bolshaya Cheremushkinskaya 25,
Moscow, 117259 Russia*

²*“Kurchatov Institut” National Research Center, pl. Kurchatova 1, Moscow, 123182
Russia*

³*Kavli IPMU, Tokyo University, Kashiwa (WPI), Japan*

Abstract — The properties of low-mass neutron stars with rigid rotation are considered. The possible evolution paths of such stars in a close binary system with mass transfer are calculated. The properties of the gamma-ray burst GRB 170817A interpreted in terms of the stripping model, a natural ingredient of which is the explosion of a low-mass neutron star — a binary component, are briefly discussed.

Key words: low-mass neutron stars, binary systems, stellar rotation

* email: <yudin@itep.ru>

INTRODUCTION

Neutron stars (NSs), along with black holes, are the final point of evolution of massive stars exploding as supernovae. They possess surprising, as yet incompletely clear properties, while the matter in their interiors is in the most extreme state of all those available in the present-day Universe. It is well known that NSs have a maximum mass lying in the range $2 \leq M/M_\odot \leq 3$ (Rhoades and Ruffini 1974; Demorest et al. 2010). High-mass NSs get rapt attention from both observers and theoreticians, because the exact maximum mass depends critically on the unknown equation of state of matter with a density exceeding the nuclear one (Haensel et al. 2007). However, NSs also have a minimum mass of $0.1M_\odot$ (see, e.g., Haensel et al. 2002). NSs of such low masses attract less attention, first, because their properties are known comparatively better: the matter inside them is in a much less extreme state than in massive NSs due to their lower density. Second, it is still unclear whether a NS of such a low mass can be obtained from the core collapse of a massive star and the subsequent supernova explosion. Apparently, this cannot be done directly. A NS can reach a minimum mass only as a result of its evolution in a close binary system of neutron stars.

Clark and Eardley (1977) were among the first who proposed and considered in detail this scenario. In their calculations two stars with masses of $1.3M_\odot$ and $0.8M_\odot$ approached each other due to the loss of angular momentum by the binary through the radiation of gravitational waves, and mass transfer from the less massive, but larger (in size) companion to the more massive one began at some instant. Having reached the minimum NS mass, the low-mass neutron star (LMNS) lost its hydrodynamic stability and exploded. This process was subsequently proposed by Blinnikov et al. (1984) as a source of short gamma-ray bursts (GRBs). In the succeeding paper by Blinnikov et al. (1990) D.K. Nadyozhin carried out one-dimensional hydrodynamic spherically symmetric calculations of the explosive disruption of a LMNS that reached its minimum mass. Surprisingly, the kinetic energy of the explosion turned out to be very close to the classical energy of a supernova explosion ~ 1 Bethe, i.e., 10^{51} erg. This led Imshennik (1992) to the formulation of a rotational supernova explosion mechanism, where a close NS binary results from the collapse and subsequent fragmentation of the core of a massive star. The evolution of such a NS binary, which ends with the explosion of its low-mass component, ultimately leads to the explosion of the entire star as a supernova. The LMNS explosion was considered

by Colpi et al. (1989) and Sumiyoshi et al. (1998), who, among other things, studied the properties of the burst of neutrino radiation accompanying the explosion and the nucleosynthesis processes. Having taken the parameters from Blinnikov et al. (1990) as initial data, Manukovskiy (2010) carried out three-dimensional self-consistent hydrodynamic calculations of the explosion of a LMNS in the orbit of a massive companion. Many historical details of the development of this scenario can be found in the review by Baklanov et al. (2016).

However, the interest in this mechanism of short GRBs decreased with time, because their observed energies were, as a rule, much greater and their spectra were harder than those predicted by Blinnikov et al. (1990) (see, e.g., Hamidani et al. (2019) and references therein). GRB 170817A associated with the signal GW170817 at the LIGO and Virgo gravitational-wave interferometers (Abbott et al. 2017a) helped to revive the interest. This GRB turned out to be peculiar: with a low isotropic energy (Abbott et al. 2017b), spectral peculiarities (Villar et al. 2017), and a large estimated ejecta mass (Siegel 2019). In addition, no traces of the presence of a strong jet were observed either (Dobie et al. 2018). All these characteristic features of GRB 170817A are difficult to explain in terms of the standard NS merger scenario, where two NSs merge into one object — a supermassive NS or a black hole. On the other hand, these features are naturally explained in terms of the Blinnikov et al. (1984) mechanism, which we will call below the stripping model.

A detailed discussion of the merger and stripping models and their comparison with observational data will be given in an appropriate place (Blinnikov et al. 2020), while here we will only note that the realizability of these scenarios is determined mainly by the initial binary mass ratio (asymmetry). A nearly vertical segment corresponds to NSs with a mass of the order of the solar one on the NS mass–radius diagram (see, e.g., Lattimer and Prakash 2001). Thus, the radius of such NSs depends weakly on their mass (an effective polytropic index $n \approx 1$), and during their merger they behave like two liquid droplets and merge into one object. Note that almost all of the calculations of this process performed to date dealt precisely with the case of equal and fairly large masses. Even in the case where a large mass ratio was considered (Dietrich et al. 2017), the mass of the less massive component was fairly large (of the order of the solar one). If, however, the mass ratio is great and the LMNS mass is fairly small, then the stripping scenario should be realized. The specific NS mass, small enough for the onset of stripping, depends on the equation of state of matter in the nuclear and, what is more important in this case, subnuclear region.

As shown by Sotani et al. (2014), there are significant uncertainties in the behavior of the LMNS mass–radius curves. However, an analysis of fig. 1 from this paper allows the characteristic value of this mass to be estimated as $M \sim 0.5M_{\odot}$. We will call NSs with masses smaller than this value low-mass ones (LMNSs).

FORMULATION OF THE PROBLEM

In most of the studies cited above the binary NS spin was neglected. To a first approximation, this is completely justified for a dense massive component. However, a LMNS has a peculiar structure: a tiny dense compact core containing the bulk of the mass and an extended envelope. The rotation effects may turn out to be important for such a structure.

We will consider the influence of the LMNS spin on its parameters and the possible evolution paths. In this case, we will neglect the tidal deformation from the massive companion by assuming the distribution of matter in the LMNS to be axisymmetric. The validity of this approximation breaks down only for the outer, least dense layers whose structure is determined by the isolines of a modified (with the LMNS spin) Roche potential. Determining the LMNS shape generally requires solving a three-dimensional problem in this case.

In addition, we will deem the LMNS rotation law to be the rigid one, i.e., will assume that the characteristic angular momentum redistribution time inside the NS is much shorter than the mass transfer time. This assumption can break down only at the final evolutionary stages of a NS binary system.

Since the original ROTAT code (for its description, see below) used by us for the calculation of rotating configurations is Newtonian, i.e., it disregards the general relativity effects, we will restrict our study to a LMNS with a mass $M \leq 0.2M_{\odot}$. The radius of such stars is $R \geq 20$ km, and the relativistic parameter turns out to be fairly small: $\frac{2GM}{Rc^2} \leq 0.03$.

The Equation of State

We will use the fits for the dependence of pressure on density $P = P(\rho)$ proposed by Haensel and Potekhin (2004) as the equations of state (EOS) of matter. They describe the properties of NS matter at temperature $T = 0$ in a wide range of densities both in the sub-nuclear region and at densities above the nuclear one. The convenient subroutines written

Table 1. Properties of minimum-mass NSs for various equations of state

EoS	M_{\min} [M_{\odot}]	R [km]	ρ_c [$\text{g} \cdot \text{cm}^{-3}$]
BSk19	0.097	208	$1.8 \cdot 10^{14}$
BSk22	0.089	272	$1.5 \cdot 10^{14}$
BSk24	0.093	238	$1.9 \cdot 10^{14}$
BSk25	0.091	233	$2.3 \cdot 10^{14}$
BSk26	0.096	222	$1.8 \cdot 10^{14}$

in FORTRAN that compute various thermodynamic quantities for several possible EOS are presented at the site of one of the authors (<http://www.ioffe.ru/astro/NSG/BSk/>). At low densities ($\rho \lesssim 3 \times 10^5 \text{ g} \cdot \text{cm}^{-3}$) these fits are inaccurate, and we smoothly join them with the $n = 3/2$ polytrope ($P = P_0 \rho^{5/3}$). The parameters of non-rotating LMNSs calculated using some of these EOS are given in Table 1. The first, second, third, and last columns provide the EOS abbreviation, the corresponding minimum mass, the radius, and the central density, respectively. Everywhere below we will use the BSk19 fit as the basic case for our calculations.

The Rotat Code

Let us briefly describe the algorithm implemented in the ROTAT code (Aksenov and Blinnikov 1994). Consider an axisymmetric stellar configuration in a state of stationary rotation. The equation of motion of a fluid element is

$$\rho(\mathbf{v}\nabla)\mathbf{v} + \nabla P + \rho\nabla\Phi = 0, \quad (1)$$

where \mathbf{v} is the velocity, ρ is the matter density, Φ is the gravitational potential that satisfies the Poisson equation

$$\nabla^2\Phi = 4\pi G\rho, \quad (2)$$

and P is the matter pressure related to the density by the barotropic equation of state

$$P = P(\rho). \quad (3)$$

For the barotropic equation of state the surfaces of constant pressure and constant density coincide, while the angular velocity of rotation $\omega(\xi)$ depends exclusively on distance ξ from the rotation axis, i.e., it is constant along the cylinders coaxial with the rotation axis

(the Poincare theorem, see Appendix A). Thus, the linear velocity of the fluid element is related to its angular velocity by the expression

$$\mathbf{v} = \xi\omega(\xi)\mathbf{e}_\varphi, \quad (4)$$

where \mathbf{e}_φ is a unit vector in the direction of the azimuthal angle φ . Integrating the equation of motion (1), we can obtain the Bernoulli integral

$$H(\rho) + \Phi + \Psi = C, \quad (5)$$

where C is the constant of integration, H is the enthalpy defined by the expression

$$H(\rho) = \int \frac{dP'}{\rho'}, \quad (6)$$

and Ψ is the centrifugal potential related to the angular velocity by the expression

$$\Psi = - \int^\xi \omega^2(\xi')\xi' d\xi'. \quad (7)$$

For rigid rotation

$$\Psi = -\frac{C_\psi}{2}\xi^2. \quad (8)$$

If we use the Bernoulli integral (5) to express the density as a function inverse to the enthalpy and substitute this into the Poisson equation (2), then we will obtain an equation containing the gravitational potential and the constants C and C_ψ . This equation is then written in finite differences on a two-dimensional grid (r, ϑ) , where r is the distance from the configuration center and ϑ is the polar angle measured from the rotation axis. The radial coordinate on the grid outside the sphere enclosing the entire star is a quantity inversely proportional to the distance to the center (Clement 1974).

The boundary conditions correspond to symmetry at the center: for $r \rightarrow 0$ we have

$$\left. \frac{\partial \Phi}{\partial r} \right|_{r=0} = 0, \quad \left. \frac{\partial^2 \Phi}{\partial r^2} \right|_{r=0} = \frac{4\pi}{3}G\rho_c, \quad (9)$$

where ρ_c is the density at the stellar center (the erratum in the original paper by Aksenov and Blinnikov (1994) in the grid form of the central condition is corrected in Appendix B). The condition $\Phi \rightarrow 0$ is specified for $r \rightarrow \infty$. In addition, the ratio of the polar and equatorial radii $\theta = R_p/R_e$ and the maximum density allow C and C_ψ to be determined simultaneously with the field Φ .

The density at each grid point can be found using (5). The position of the grid point at which the maximum density is reached can be found during the calculations. Owing to the use of the differential relation (2) between the gravitational potential and density instead of the integral expression for the potential via the density, the matrix of coefficients for the system of difference equations is sparse, i.e., there are many zero elements in it. The system of difference equations was solved by the quadratically converging Newton method. In this case, we used the method of solving a system of linear equations (obtained by linearizing the complete system in the Newton method) with sparse matrices of coefficients described in the book by Osterby and Zlatev (1983). The accuracy of our calculations was checked by the virial test

$$VT = \frac{1}{|W|} \left| 2T + W + 3 \int P dV \right|, \quad (10)$$

where T is the rotational kinetic energy of the star and W is its gravitational energy.

RESULTS OF OUR CALCULATIONS

The main results of our calculations are presented in Fig. 1. It shows the lower part of the mass–radius (M – R) diagram for LMNSs. In the inset the central part of the figure is shown on an enlarged scale. The dash–dotted lines bounding the narrow horn-shape region correspond to configurations with fixed oblateness $\theta \equiv R_p/R_e$, where R_p and R_e are the polar and equatorial radii, respectively. Everywhere below the parameter R on the diagram is equal to the equatorial radius R_e of the star. Naturally, $\theta = 1$ corresponds to non-rotating stars. On the other side the region of our configurations is bounded by (approximate) $\theta = 2/3$. We failed to obtain more oblate configurations with rigid rotation. The reason is explained in detail in Appendix A. Here we will only say that at these values of θ a mass outflow from the equator begins in rigidly rotating LMNSs. Thus, all of the admissible configurations are contained in the narrow band between the $\theta = 1$ and $\theta = 2/3$ curves. These results are also in complete agreement with the conclusions by Haensel et al. (2002).

Let us now consider the possible evolution paths of a LMNS in a binary system. The dashed lines indicate the configurations with a constant total angular momentum ($J = \text{const}$). If the star could lose its matter without any change in J (for example, in the form of a circumpolar outflow or a jet), then its evolution on the (M – R) diagram would be described by one of the dashed curves in the direction indicated by the arrows. Each

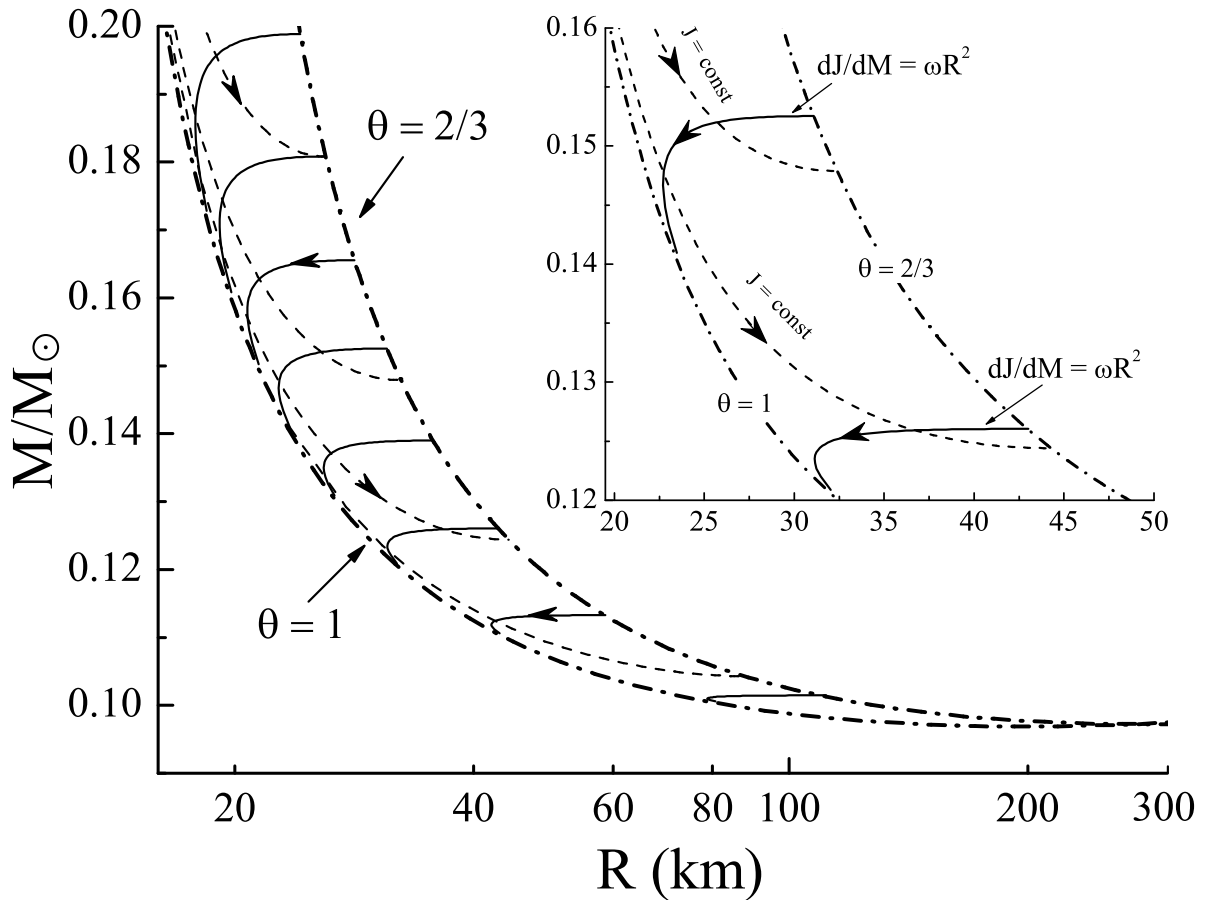


Fig. 1. LMNS mass–radius diagram. The dash–dotted lines bounding the horn-shaped region correspond to the sequence of nonrotating configurations with $\theta = 1$ and configurations with fixed oblateness $\theta = 2/3$. The dashed lines give the sequence of stars with a constant total angular momentum J . The solid lines correspond to the law of evolution $dJ/dM = \omega R^2$. For the remaining details, see the text.

such curve begins almost tangentially from the $\theta = 1$ line and gradually approaches the equatorial outflow limit $\theta = 2/3$. However, this evolution path looks unrealistic.

Let us now turn to a more likely scenario: a LMNS in a binary system fills its Roche lobe and begins to transfer its mass to the more massive companion. In this case, matter outflows virtually from the equator. Depending on the orientation of the LMNS spin axis relative to the orbital plane, the outflow point can lie not exactly on the equator. Here we will restrict ourselves to the simplest case of an equatorial outflow. The star will then lose not only its mass, but also its angular momentum. It is easy to show that this will occur in accordance with the law

$$\frac{dJ}{dM} = \omega(R_e)R_e^2, \quad (11)$$

where ω is the angular velocity of rotation, which is constant over the star in the case of

rigid rotation considered by us, though, of course, it changes during star’s motion across the $(M-R)$ diagram. The corresponding trajectories are indicated by the solid lines with arrows. As we see, the evolution path is nontrivial in this case: initially the star moves leftward across the mass–radius diagram, rapidly losing its angular momentum, with the change in mass being comparatively small. As the $\theta = 1$ line of non-rotating configurations is approached, the stellar track turns and begins to asymptotically approach it, moving downward and rightward. Thus, the LMNS evolution in the binary system actually breaks up in this case into two stages: at the first stage, it loses its angular momentum and its radius decreases; at the second stage, its evolution is virtually indistinguishable from the evolution of non-rotating configurations: the radius increases rapidly as the mass is lost.

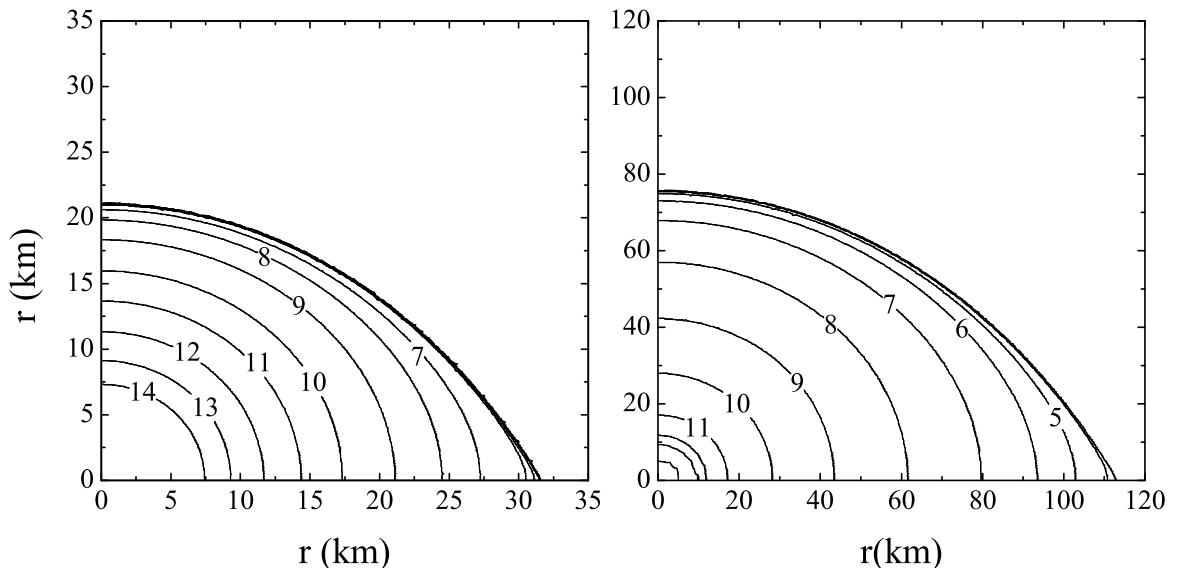


Fig. 2. Spatial structure of critically ($\theta = 2/3$) rotating stars with masses $M = 0.15M_{\odot}$ (left) and $M = 0.1M_{\odot}$ (right). Density isolines are shown; the numbers correspond to $\lg \rho \text{ g/cm}^3$. The three central lines for the star with $M = 0.1M_{\odot}$ correspond to $\lg \rho = 12, 13$ and 14 ; the corresponding numbers are not shown lest the graph be overloaded.

Let us discuss two more questions. First, consider the structure of a LMNS with critical rotation. Figure 2 shows the structure of LMNSs with oblateness $\theta = 2/3$ and masses $M = 0.15M_{\odot}$ (left) and $M = 0.1M_{\odot}$ (right). The curves with numbers are isolines of the logarithm of density $\lg \rho \text{ (g/cm}^3\text{)}$. On the right panel the central lines correspond to $\lg \rho = 12, 13, 14$; the corresponding numbers are not plotted lest the figure be overloaded. As we see, the star consists of a tiny dense nearly spherical core and an extended deformed envelope (cf. the discussion in Haensel et al. (2002)). In the case of $M = 0.1M_{\odot}$, the

contrast between the size of the core containing the bulk of the mass and the envelope size is particularly striking.

The configurations with critical rotation were checked for stability in accordance with the criterion developed in the paper by Bisnovatyi-Kogan and Blinnikov (1974). More specifically, for each configuration we constructed a series of models preserving the angular momentum distribution $j(m) = \omega(\xi)\xi^2$ from the dimensionless mass coordinate inside the star $m = M(\xi)/M_s$, where ξ is the cylindrical radius (cylindrical coordinate) and M_s is the total mass of the star. The following condition should be fulfilled for the configuration to be stable:

$$\left(\frac{\partial M}{\partial \rho_c}\right)_{j(m)} > 0, \quad (12)$$

where ρ_c is the central density and the derivative in (12) is taken along the series of models. All of the stellar configurations considered turned out to be stable. This is not surprising, because the hydrodynamic stability of LMNSs is determined mainly by the properties of their massive cores. However, even the critical rotation for their envelopes turns out to be extremely weak for the central stellar regions. The mass outflow from the equator begins much earlier than the hydrodynamic stability is lost. However, the situation can change under differential rotation, in the case where the core rotates much faster than the envelope (see also Appendix A). This question requires a special consideration; we are planning to carry out an appropriate study in the immediate future.

The second question that should be discussed are the properties of LMNSs with rotation in the region of the minimum mass. Figure 3 shows the lower part of the LMNS mass–radius diagram on an enlarged scale. Two limiting curves are plotted: the $\theta = 1$ curve without rotation and the $\theta = 2/3$ curve with critical (in the sense of an outflow) rotation. This region of the diagram is particularly interesting, because here the LMNS loses its stability and experiences an explosive expansion (Blinnikov et al. 1990). Accordingly, rotation can affect the point of stability loss and, hence, the explosion parameters. Figure 3 shows that the minimum mass changes (increases) insignificantly even for the case of critical rotation. The radius of the last stable non-rotating configuration is slightly more than 200 km (see Table 1), while for the rotating one it is ~ 300 km. Given that θ is $2/3$ here, this increase in the radius is explained simply by the deformation of the light extended envelope. It can be concluded that rigid rotation affects insignificantly the properties of the lower NS mass limit and, hence, the parameters of the explosion following the loss of

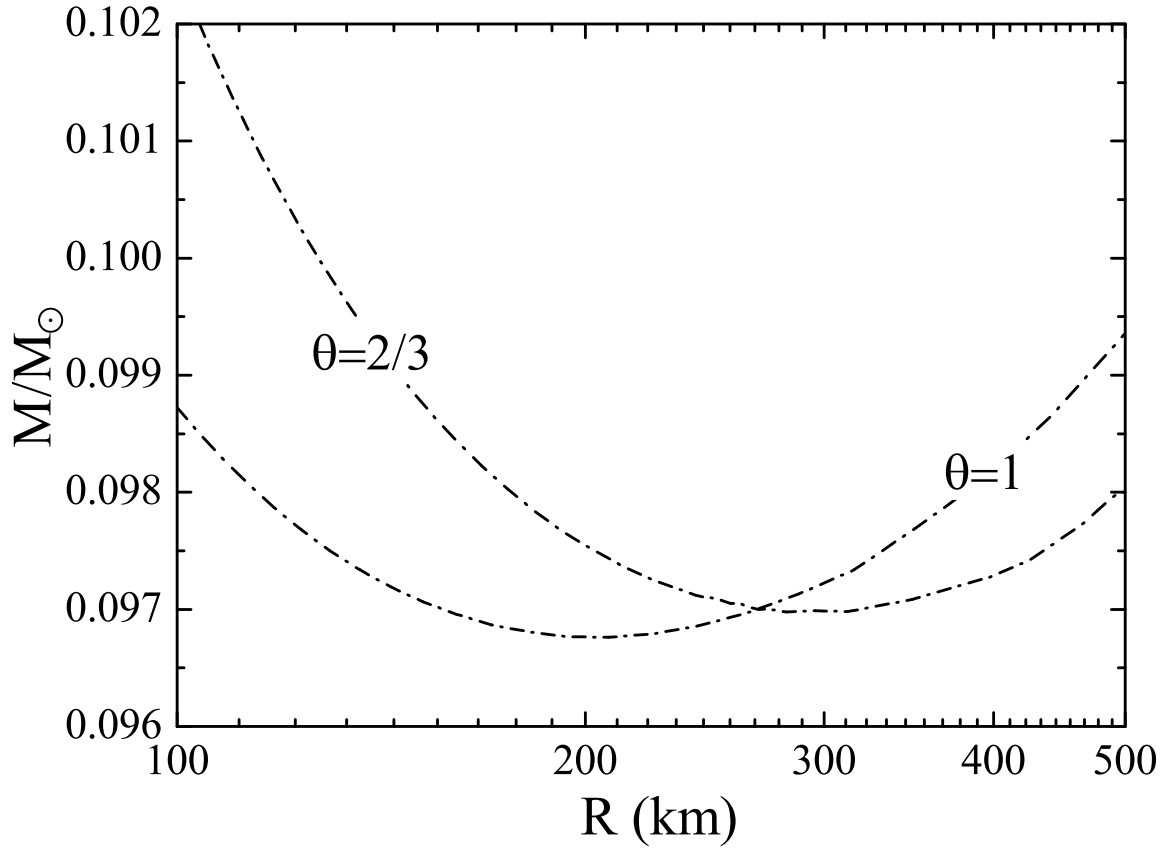


Fig. 3. Region of the NS mass–radius diagram near the minimum. The lines of non-rotating, $\theta = 1$, and critically rotating, $\theta = 2/3$, configurations are shown.

LMNS stability.

CONCLUSIONS

Let us list and discuss the main results of this paper. First, we showed that all of the admissible states of rigidly rotating LMNSs occupy a comparatively narrow region (Fig. 1) bounded by the curves with constant oblateness on the mass–radius diagram: $\theta = 1$ (non-rotating configurations) and $\theta = 2/3$. The reason why the latter value was singled out is explained in Appendix A. All configurations in the region under consideration (“horn”) turn out to be hydrodynamically stable, while a mass outflow from the equator begins in the star as the $\theta = 2/3$ line is approached (Fig. 2, which shows the structure of several critical configurations). Second, we showed (Fig. 3) that rigid rotation affects weakly the minimum NS mass. This conclusion seems important from the viewpoint of studying the conditions accompanying the loss of LMNS stability and the ensuing processes.

However, we deem the derived evolution paths (the solid curves in Fig. 1) corresponding to the loss of mass by the star from the equator to be the most important result. This course of events seems most probable in the case of mass transfer in a close NS binary. Two NSs approach each other due to the loss of angular momentum through gravitational radiation. Let us first consider the case of a non-rotating LMNS: during the approach it is the first to fill its Roche lobe. As soon as part of its mass is transferred to the more massive companion, the separation between the stars increases, because the binary becomes more asymmetric. However, the LMNS radius also increases (Fig. 1). Hence, two cases can be realized: at a sufficiently large LMNS mass this increase in its radius is not enough for the accretion to continue, and the binary should again lose its angular momentum due to gravitational radiation before a new mass transfer. Thus, the evolution of the binary at this stage will be governed precisely by the (slow) radiation of gravitational waves. If, alternatively, the LMNS mass is sufficiently small, then its radius increases faster than the components fly apart, and the binary will evolve on the hydrodynamic (fast) time scale.

Let us now consider the case of mass transfer in a binary with a LMNS that has a fairly strong rotation. The LMNS evolution will take the path indicated in Fig. 1 by the solid lines in the direction of the arrows. Thus, its radius will drop until the LMNS loses almost all of its angular momentum! This means that during all of this period the binary evolution rate will be determined by the slow energy loss through gravitational radiation. Only having gotten rid of the rotation almost completely does the LMNS track turn and asymptotically approach the $\theta = 1$ line of non-rotating configurations. Subsequently, its evolution differs little from that for a star without rotation. Thus, the LMNS spin can only lengthen the evolution time of a NS binary system, but the LMNS approaches the minimum mass virtually non-rotating and, hence, the parameters of its explosion, which marks the loss of stability by it, will be the same as those in the absence of rotation. This conclusion seems particularly important to us.

The work of A.V. Yudin and S.I. Blinnikov was supported by the Russian Foundation for Basic Research (project no. 18-29-021019 mk).

APPENDIX A: MAXIMUM OBLATENESS IN THE ROCHE MODEL

Let us describe the reason why the limiting LMNS oblateness is close to $2/3$ (see also Krat 1950). Consider a rotating axisymmetric star. The equilibrium equations will be written

as (Tassoul 1978)

$$\frac{1}{\rho} \frac{dP}{d\xi} = -\frac{d\varphi_G}{d\xi} + \omega^2 \xi, \quad (1)$$

$$\frac{1}{\rho} \frac{dP}{dz} = -\frac{d\varphi_G}{dz}. \quad (2)$$

Here, P is the pressure, ρ is the matter density, φ_G is the gravitational potential, and ω is the angular velocity of rotation. Equation (1) describes the equilibrium of matter in a plane perpendicular to the rotation axis, $\xi = \sqrt{x^2 + y^2}$ is the cylindrical radius. In the analogous Eq. (2) z is the coordinate along the rotation axis. Suppose that the equation of state is barotropic, i.e., $P = P(\rho)$ (this is definitely the case for a cool NS considered by us). Then, introducing the enthalpy

$$H(\rho) \equiv \int \frac{dP'}{\rho'}, \quad (3)$$

and integrating Eq. (2), we will obtain $H + \varphi_G = F(\xi)$, where $F(\xi)$ is some function. Substituting this expression into (1), we will obtain the Poincare theorem on the constancy of the angular velocity on cylindrical surfaces coaxial to the rotation, $\omega = \omega(\xi)$, and the explicit form of the function $F(\xi)$ itself:

$$F(\xi) = H + \varphi_G = \int \omega^2 \xi d\xi + \text{const.} \quad (4)$$

In the Roche model the entire mass is concentrated at the center, and the gravitational potential can be specified in explicit form: $\varphi_G = -\frac{GM}{r}$. LMNSs have a tiny dense core, where almost all of their mass is concentrated, and an extended tenuous envelope (see, e.g., Fig. 2). Therefore, the Roche model must well describe our case, at least to a first approximation. Let the equatorial and polar radii of the star be R_e and R_p , respectively. From (4) we then obtain

$$\int_0^{R_e} \omega^2 \xi d\xi = \varphi_G(R_e) - \varphi_G(R_p) = GM \left(\frac{1}{R_p} - \frac{1}{R_e} \right). \quad (5)$$

Under critical rotation a mass outflow from the equator begins in the star, i.e., the following condition is fulfilled:

$$\omega^2(R_e) R_e = \frac{GM}{R_e^2}. \quad (6)$$

Let us introduce the dimensionless quantities $\varpi \equiv \omega(\xi)/\omega(R_e)$ and $\zeta = \xi/R_e$. Relation (5) will then be written as

$$\frac{R_e}{R_p} = 1 + \int_0^1 \varpi^2(\zeta) \zeta d\zeta, \quad (7)$$

with the constraints

$$\varpi(1) = 1, \quad \frac{d\varpi(\zeta)\zeta^2}{d\zeta} \geq 0. \quad (8)$$

The latter Solberg–Hoiland condition provides the rotation stability (for more details, see Tassoul 1978). For rigid rotation $\varpi = \text{const}$, and we get $R_e/R_p = 3/2$, which is what was required to prove. The widely used rotation law, which, given the normalization, is written as $\varpi(\zeta) = (1 + \alpha)/(1 + \alpha\zeta^2)$, where α is some positive constant, leads to the ratio $R_e/R_p = (3 + \alpha)/2$. Thus, generally speaking, differentially rotating LMNS can be more oblate, up to $\theta = R_p/R_e < 2/3$.

APPENDIX B: THE CENTRAL BOUNDARY CONDITION IN THE ROTAT CODE

The boundary conditions correspond to symmetry at the center: for $r \rightarrow 0$ we have

$$\int_0^\pi \nabla^2 \Phi \sin \vartheta d\vartheta \rightarrow 3 \int_0^\pi \frac{\partial^2 \Phi}{\partial r^2} \sin \vartheta d\vartheta, \quad (1)$$

so that

$$\begin{aligned} 4\pi G\rho_c &= \left. \frac{1}{2} \int_0^\pi \nabla^2 \Phi \sin \vartheta d\vartheta \right|_{r=0} \\ &\simeq \frac{6}{(\Delta r)^2} \sum_k \left\{ \cos[\max(0, \Delta\vartheta(k - 1/2))] \right. \\ &\quad \left. - \cos[\min(\pi/2, \Delta\vartheta(k + 1/2))] \right\} (\Phi_{1,k} - \Phi_{0,k}), \end{aligned} \quad (2)$$

where we use the notation $\Phi_{i,k} \equiv \Phi(r_i, \vartheta_k)$, and the summation over k to take the integral (1) is from the pole to the equator. The coefficient 6 in the last equation is derived from the product of 3 in (1) and 2 in the approximation of the second derivative with respect to the radius at the center:

$$\frac{\partial^2 \Phi}{\partial r^2} = 2 \frac{\Phi_{1,k} - \Phi_{0,k}}{(\Delta r)^2}. \quad (3)$$

REFERENCES

1. *Abbott B.P. et al.*, *Astroph. J. Lett.*, **848** L:12, (2017a)
2. *Abbott B.P. et al.*, *Astroph. J. Lett.*, **848** L:13, (2017b)
3. *Aksenov A.G., Blinnikov S.I.*, *Astron. & Astrophys.*, **290**, 674–681 (1994)
4. *P.V. Baklanov, S.I. Blinnikov, K.V. Manukovskiy, D.K. Nadyozhin, I.V. Panov, V.P. Utrobin, and A.V. Yudin*, *Phys. Usp.* 59, 796 (2016)
5. *Bisnovatyi-Kogan G.S., Blinnikov S.I.*, *Astron. & Astrophys.*, **31**, 391–404 (1974)
6. *S.I. Blinnikov, D.K. Nadyozhin, and A.V. Yudin*, *Phys. At. Nucl.* (2020, in preparation).
7. *Blinnikov S.I., Novikov I.D., Perevodchikova T.V., Polnarev A.G.*, *Sov. Astron. Lett.* **10** 177 (1984)
8. *Blinnikov S.I., Imshennik V.S., Nadyozhin D.K., Novikov I.D., Perevodchikova T.V., Polnarev A.G.*, *Sov. Astron.* 34 595 (1990)
9. *Clark J.P.A. and Eardley D.M.*, *Astroph. J.* **215** 311–322 (1977)
10. *Clement M.J.*, *Astroph. J.*, **194**, 709-714 (1974)
11. *Colpi M., Shapiro S.L. and Teukolsky S.A.*, *Astroph. J.*, **339**, 318–338 (1989)
12. *Demorest P.B., Pennucci T., Ransom S.M. et al.*, *Nature* 467, 1081 (2010)
13. *Dietrich T., Ujevic M., Tichy W., Bernuzzi S., Brüggmann B.*, *Phys. Rev. D*, **95**, 2, (2017)
14. *D. Dobie, D. L. Kaplan, T. Murphy, et al.*, *Astrophys. J. Lett.* 858, 15 (2018).
15. *Haensel P., Zdunik J.L., Douchin F.*, *Astron. Astrophys.*, **385**, 301-307 (2002)
16. *Haensel P., Potekhin A.Y., and Yakovlev D.G.*, “Neutron Stars 1 (Equation of State and Structure)” Springer, 619 (2007)
17. *Haensel, P. and Potekhin A.Y.*, *Astron. Astrophys.*, **428**, 191-197 (2004)
18. *Hamidani H., Kiuchi K., Ioka K.*, *Mon. Not. R. Astron. Soc.* 491, 3192 (2019).
19. *Imshennik V.S.* *Sov. Astron. Lett.* **18**, 194 (1992)
20. *V.A. Krat*, “Equilibrium Figures of Celestial Bodies”, (Gos. Izdat. Tekh.-Teor. Liter., Moscow, Leningrad, 1950) [in Russian].

21. *Lattimer J.M., Prakash M.*, *Astrophys. J.*, **550**, 426 (2001)
22. *Manukovskiy K.V.*, *Astron. Lett.* **36**, 3, 191–203 (2010)
23. *O. Osterby and Z. Zlatev*, “Direct Methods for Sparse Matrices” (SIAM, Philadelphia, 1986).
24. *Rhoades C.E., Ruffini R.*, *Phys. Rev. Lett.*, **32**, 6, pp. 324-327 (1974)
25. *Sotani H., Iida K., Oyamatsu K., Ohnishi A.*, *Prog. Theor. Exp. Phys.*, **2014**, 5 (2014)
26. *Sumiyoshi K., Yamada S., Suzuki H., Hillebrandt W.*, *Astron. Astrophys.* **334**, 159–168 (1998)
27. *Siegel D.M.*, *Eur. Phys. J. A* 55, 203 (2019).
28. *J.-L. Tassoul*, “Theory of Rotating Stars” (Princeton Univ. Press, Princeton, 1978; Mir, Moscow, 1982).
29. *Villar V.A., Guillochon J., Berger E. et al.*, *Astroph. J. Lett.*, 851:L21 (2017)